Journal of Molecular Modeling (2022) 28: 121
https://doi.org/10.1007/s00894-022-05083-1

ORIGINAL PAPER

Long-range parameter optimization for a better description of potential energy surfaces using Density Functional Theory

Matheus de Oliveira Bispo[1] · **Demétrio Antônio da Silva Filho**[1]

Received: 7 December 2021 / Accepted: 8 March 2022 / Published online: 15 April 2022

Abstract

The advance of computing and the development of modern quantum chemistry models such as Density Functional Theory (DFT) have allowed scientists to perform fast in silico studies with accurate results. It also allowed for the achievement of empirically unattainable quantities such as Potential Energy Surfaces (PES), a fundamental construct in various applications, such as the study of weakly bound systems. One of DFT's current weaknesses is a reliable description of PESs, due to a lack of suitable exchange-correlation functionals. In general, other post-Hartree-Fock methods are employed, such as *n*th-order Møller-Plesset's Perturbation Theory (MPn) or Coupled Cluster Theory (CCSD(T)) with large basis sets. Despite producing good results, these methods demand much computational power when applied to large systems. This work presents a novel approach of PES description of the H_2O_2–Kr system using DFT by optimizing a long-range parameter present in some DFT functionals, obtaining results similar to those of the MPn methods with somewhat less computational time necessary.

Keywords Potential energy surface · Density Functional Theory · Long-range parameter

Introduction

The Potential Energy Surface (PES) of a molecular system is a core concept of atomic and molecular physics. A PES shows how potential energy varies with respect to the system's geometric degrees of freedom. It governs every atomic nucleus's dynamics, dictating how they vibrate, rotate and translate in space [1]. It can also describe reaction paths [2] and regions of possible stable and unstable molecular structures, as well as be used in the calculation of several spectroscopic [3] and thermodynamic [4] properties of a molecular system.

In the context of weakly bounded systems, such as those in the interstellar medium, properties derived from PES can be more easily compared to their corresponding experimental results [5]. Therefore, it is crucial to study this type of systems, especially when applied to astronomical sciences.

Given the great importance of a PES in studying a molecular system, an accurate description of this surface is key to deriving important properties that can be compared with experimental results [2–4]. For this matter, the description of PESs for small molecules can be done using post-Hartree-Fock methods such as *n*th-order Møller-Plesset Perturbation Theory (MPn) [6–9] or Coupled Cluster Theory (CCSD(T)) [9, 10], along with large basis sets such the Dunning basis [11]. The data acquired is then fitted to an analytical form in order to study molecular dynamical properties of the system [6].

Such methods require more time and computational resources to evaluate the energy corrections of post-HF, even when considering small molecules. For instance, when studying collision dynamics of molecules such as propylene oxide [9, 12], the concept of PES becomes less effective due to the increased dimensionality of the hypersurface. As such, a full description is compromised and, instead, the PES is restricted to only some degrees of freedom.

On the other hand, Kohn-Sham (KS) Density Functional Theory (DFT) adopts a different approach by considering the energies and operators as functionals of the electron density $\rho(\vec{r})$ [13]. This approach reduces the dimensionality

This article belongs to the Topical Collection: *XXI-Brazilian Symposium of Theoretical Chemistry (SBQT2021)*

✉ Demétrio Antônio da Silva Filho
dasf.all@gmail.com

Matheus de Oliveira Bispo
matheus.physis@gmail.com

[1] Physics Institute, University of Brasilia, 70910-900, Brasilia, Federal District, Brazil

of the problem from $3N$ variables to just 3 (N being the number of electrons) and makes calculations faster [14]. Despite the fact that some exchange-correlation functionals describing optical and electronic properties of several molecular systems [15–18] successfully, there is an absence of appropriate functionals that can reproduce the theoretically accurate MPn results for PESs [10].

The exchange-correlation functional $E_{xc}[\rho(\vec{r})]$, a key component of KS-DFT, is often approximated using a plethora of different methods [19]. As an example of the latter, a particular class known as long-range corrected (LRC) hybrid density functionals, introduces a range separation parameter ω that splits and modulates short- and long-range interactions as follows [20]:

$$\frac{1}{r} = \underbrace{\frac{\mathrm{erfc}(\omega r)}{r}}_{SR} + \underbrace{\frac{\mathrm{erf}(\omega r)}{r}}_{LR}, \tag{1}$$

The long-range parameter ω modulates the distance where the range separation occurs. The lower the value of ω, the farther this separation occurs. Usually, LR interactions are modeled by HF exchange and correlation, while the hybrid, semi-local exchange-correlation energies model the SR interactions [21]. The substitution indicated in (1) is done directly in the KS hamiltonian.

This class of functionals initially gained notoriety for its implementation in correcting the HOMO-LUMO gap calculations in organic materials [18]. Their respective default ω values were determined by optimizing each LRC functional against a training set of different molecular systems in order to obtain more accurate thermochemical and kinetic properties in mind [20, 22].

Since then, ω optimization has been used for calculating optical properties [15–17] and binding energies [23] of molecular systems. However, in principle, the ω parameter could be tuned to fit an existing MPn reference PES via optimization algorithms.

The present work aims to analyze ω optimization as an alternative solution for the construction and description of PESs for weakly bound systems. We compare the results using both the default and optimized parameters with the reference calculations using MP4, with the goal of obtaining results similar to those of perturbative methods while requiring less computational time.

Methodology

System geometry

The system of interest for this work consists of a hydrogen peroxide molecule (H_2O_2) and a krypton atom (Kr), as shown in Fig. 1. Not only is H_2O_2 a simple molecule, but it is also the smallest molecule in nature to present chirality [8, 24]. Besides, its PESs are already well characterized and adjusted to an analytical form [6].

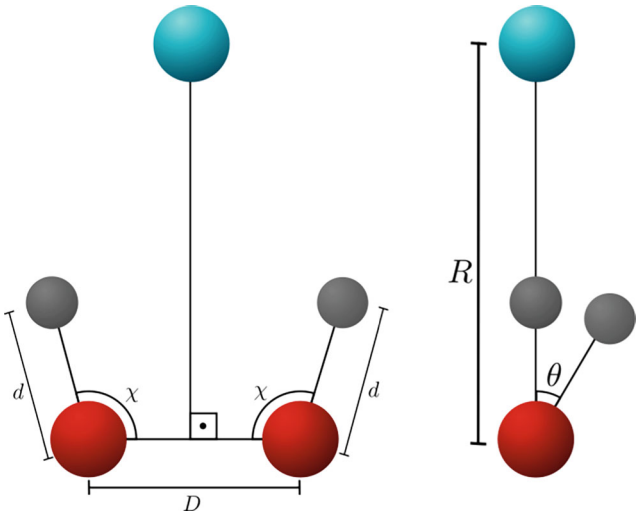

Fig. 1 Studied system comprised of a Kr atom (above, in blue) and a H_2O_2 molecule (below), where the oxygen atoms are in red and the hydrogen atoms are in gray. The fixed parameters D, d, χ are shown, as well as the variables R and θ

We performed a rigid scan on the system using the Gaussian 16 software [25], where the fixed parameters were the $O-O$ and $H-O$ distances $D = 1.450$, Å and $d = 0.966$, Å, respectively, as well as the angle of incidence, set to 90^o. This was done to reduce the system's dimensionality and make comparisons with previous studies [6].

Only the dihedral angle θ, defined as the angle between the two planes defined by the $H-O-O$ bonds, and the distance R between the Kr atom and the $O-O$ bond's midpoint were the variables of interest of our PES scan. These variables' values ranged between 0^o and 360^o with a step of 10^o, and 3 Å and 5 Å with a step of 0.1 Å, respectively.

The reference method used was the MP4 method, using the aug-cc-pVTZ basis set. As is typical with this basis set, we used the counterpoise correction to avoid the basis set superposition error. This combination of method and basis set has a good track record in producing reliable PESs [6–8].

The DFT calculations also used the same basis sets, and the ωB97XD [20], the LC-BLYP [26], and the LC-ωPBE [22] functionals were tentatively optimized. These functionals were chosen for their previous use in a related study [10].

ω optimization procedure

For the optimization procedure to be computationally viable, an important assumption was made: for each

LRC-DFT functional, there is a unique optimal, geometry-independent long-range parameter ω such that the PES scanned using it has the closest possible qualitative and quantitative properties to the reference PES.

The upside of this approach is that, once the ω parameter is optimized, no further MP4 calculations are necessary. Therefore, one uses only DFT calculations with that optimized ω value for every new point outside the reference range.

We computed the PES with an LRC-DFT functional and a specific ω value. The same nuclear configurations were used for MP4 and DFT PESs. Once the scan is completed, the energy values of each and every nuclear configuration were compared with the corresponding reference values via a predetermined error metric.

This way, the idea of optimizing functionals is, therefore, translated into minimizing the discrepancy Δ between the reference and DFT PESs. In order to perform this minimization, we used the Nelder-Mead [27] algorithm for its simplicity and ease of implementation. In the present work, we used the Mean Square Error (MSE), which returns the root mean squared of the energy difference:

$$\Delta_{MSE} = \sqrt{\frac{1}{MN}\sum_{i=1}^{N}\sum_{j=1}^{M}(E_{ij}^{MP4} - E_{ij}^{DFT})^2}, \quad (2)$$

where $N = 21$ is the number of radial points and $M = 36$ is the number of angular points.

For the ω optimization scheme described above, a Python program was developed using the `numpy` [28] and `scipy` [29] libraries. Additionally, we used the `matplotlib` [30] library for the plots, and the `os` library to integrate the Python program with the Linux operating system's shell and the Gaussian 16 software [25]. All programs and scripts used here are available publically in an online repository.

Results and discussion

MP4 Theory

By the end of MP4 calculations, the PES in Fig. 2 was obtained. In order to facilitate comparisons, the remainder of the graphs shown in this article will consist of cross-sections of the PES taken along the R axis, with $\theta = 0^o$ fixed, and the θ axis, with $R = 3.5$ Å fixed. We will compare the minima of both curves with their respective DFT counterparts, as these points are relevant in several applications of a PES [3, 6].

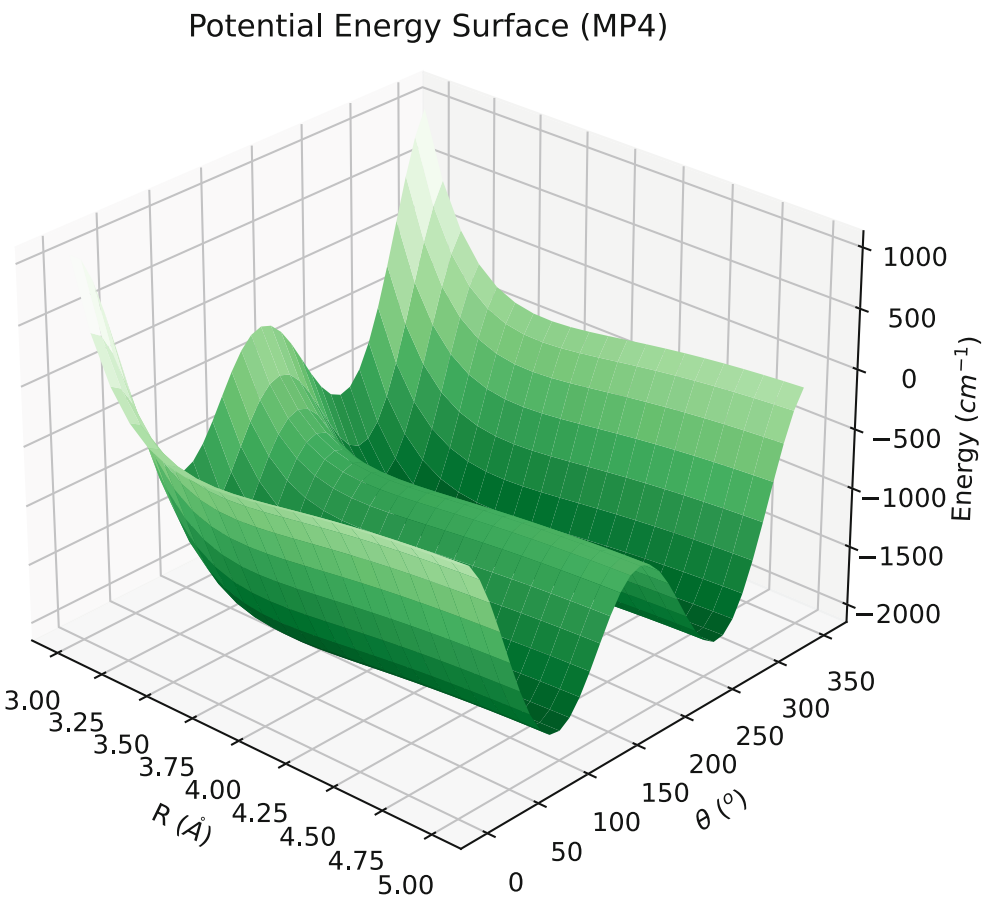

Fig. 2 PES of the H_2O_2–Kr system with MP4/aug-cc-pVTZ level

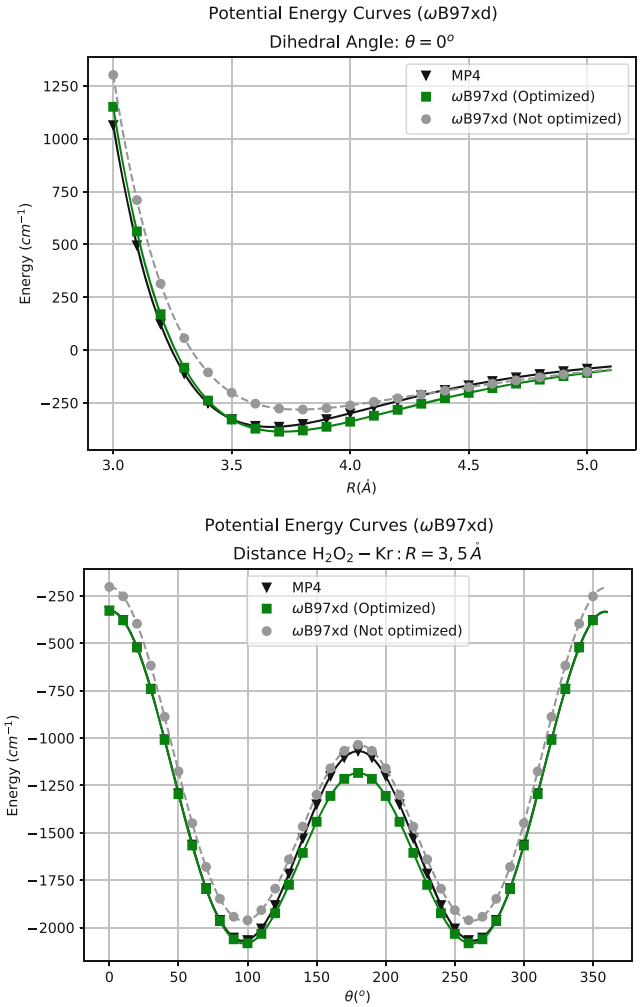

Fig. 3 Radial (above) and angular (below) potential energy curves of the H_2O_2–Kr system with ωB97xd/aug-cc-pVTZ calculation level with and without ω optimization via MSE minimization compared with the MP4/aug-cc-pVTZ level PEC

Typical behavior for interatomic potentials can be readily observed in the radial curve: the energy rapidly increases as the nuclei approach each other and, when they are far apart, the energy approaches a fixed energy value (which was taken to be 0 for $\theta = 0^o$, like all other potential surfaces raised in this work). Between these asymptotic regions, an equilibrium position at $R_e = 3.667$Å can be found, whose associated energy is $D_e = 363.768\ \text{cm}^{-1}$. These values were estimated using an interpolated univariate spline algorithm used for constructing the PEC plots.

For the angular section, the results obtained also agree with similar results in the literature [6]. It is a symmetric, periodic curve with two prominent energy barriers at the cis ($\theta = 0°$) and trans ($\theta = 180°$) configurations of the hydrogen peroxide molecule. Also, two potential wells are present at $\theta = 100°$ and $\theta = 260°$.

Optimized DFT

ωB97xd

After carrying out the electronic structure calculations using the ωB97xd functional with the default $\omega = 0.20\ \text{Bohr}^{-1}$ and optimized $\omega = 0.25\ \text{Bohr}^{-1}$ value for the same set of nuclear configurations as the reference PES, it is possible to compare both the optimized (continuous lines) and non-optimized (dashed lines) PECs present in Fig. 3, as well as the reference PECs (in black).

Overall, there is a very noticeable change in behavior on the optimized radial curve compared to the non-optimized one, especially in the short-range, with very minimal deviation past R_e. In Table 1, the equilibrium positions R_e and dissociation energies D_e of the radial PECs are compared. As expected, the optimized curve's value of R_e

Table 1 Equilibrium positions R_e and dissociation energies D_e from the radial PEC (with fixed $\theta = 0°$), as well as energy barriers and wells for the angular PEC (with fixed $R = 3.5$Å) and Mean Square Error (MSE) obtained using ωB97xd/aug-cc-pVTZ level calculation before and after optimization, along with their respective reference values

ωB97xd	Non-optimized	Optimized	Reference (MP4)
Radial curve			
R_e(Å)	3.781	3.715	3.667
D_e (cm^{-1})	281.534	386.132	363.768
Angular curve			
Cis barrier (cm^{-1})	−201.923	−328.422	−326.920
Cis well (cm^{-1})	−1963.828	−2084.677	−2070.256
Trans barrier (cm^{-1})	−1035.049	−1183.820	−1068.637
Trans well (cm^{-1})	−1963.828	−2084.677	−2070.256
Error metric (complete PES)			
MSE (10^2cm^{-1})	0.946	0.697	–

is closer to the reference value than the non-optimized one.

In general, the non-optimized curve has a shallower well compared to the reference curve, which is expected for LRC functionals [10]. This underbinding of the system was corrected during ω optimization. Likewise, the angular curve was perfectly fit around the cis configuration. On the other hand, around the trans barrier, the absolute value of the energy difference was slightly more significant between the reference curve and the optimized curve than the non-optimized curve. These results are more quantitatively displayed in Table 1.

LC-BLYP

By repeating the same procedures of the previous functional, it is possible to compare both the optimized $\omega = 1.35$ Bohr^{-1} and non-optimized $\omega = 0.47$ Bohr^{-1} PECs for the LC-BLYP functional, both of which are present in Figure S1 as well as the reference PECs.

Once again, an improved description of the radial potential can be noted, especially around the minimum at $R = 3.6$ Å. For example, comparing the equilibrium positions R_e and dissociation energies D_e of the three curves in Table S1, the discrepancy in both R_e and D_e of the optimized curve were lowered significantly in comparison to the non-optimized one.

Also, with the values in Table S1, we noticed the behavior of the angular curve improved noticeably, adjusting itself perfectly around the cis configuration. However, for points around the trans configuration, the optimized curve approached the non-optimized curve's behavior much more than the reference one.

LC-ωPBE

By repeating once more the same procedures of the previous functional, it is possible to compare both the optimized $\omega = 0.55$ Bohr^{-1} and non-optimized $\omega = 0.6$ Bohr^{-1} PECs for the LC-BLYP functional, both of which are present in Figure S2 together with the reference PECs.

This functional had much worse performance on the radial curve, staying almost the same as its non-optimized counterpart, as we compare the equilibrium positions and dissociation energies in Table S2. Similarly, comparing the results in Table S2, the angular curve had unsatisfactory results in the cis configuration. However, the trans configuration was well adjusted.

Out of the three functionals analyzed, this one developed poorly, and its use in optimized LRC-DFT is impractical. This low performance is due to the LC-ωPBE functional not fully contemplating the dispersion energy, which is heavily accounted for in this weakly bound system [8].

Conclusions

Expecting to find alternative methods for obtaining PESs, an MP4/aug-cc-pVTZ level PES was constructed for reference, and an optimization program for long-range parameter tuning of range-separated DFT functionals was developed in order to reproduce MP4 level results.

In general, our results show that ω optimization can improve DFT results, provided a single ω value can optimize an entire PES. The functionals had an acceptable overall performance: in particular, ωB97xd had the best fit to the reference PES after the optimization. The non-optimized ωB97xd underbound the system, and that underbinding was corrected during ω optimization.

LC-BLYP had a mildly successful optimization, coming in second place. Unlike ωB97xd and other LRC functionals [10], it overbound the system prior to the procedure, and afterwards, it was partially corrected. Unfortunately, LC-ωPBE showed poor results in comparison. This was due to the absence of dispersion corrections in this functional, which are heavily accounted for in weakly bound systems [8].

Qualitatively speaking, the computational time and effort of the ω optimization were sufficient to recommend its usage. Even though some applications require more precise and accurate results that justify the longer, more expensive calculations of post-HF methods, the optimized LRC-DFT can still be viable for on-the-fly calculations involving points near the minima, provided the optimization is done a priori.

This consideration, along with lower computational resource usage, promotes optimized LRC-DFT as a more viable alternative to regular DFT, expanding the range of possible methods for PES descriptions of weakly bound systems. On the other hand, this research paves the way for different functionals, minimization algorithms, and molecular systems to be studied in the future under the same goal of long-range optimization for PES descriptions.

Supplementary Information The online version contains supplementary material available at https://doi.org/10.1007/s00894-022-05083-1.

Acknowledgements M. O. B. and D. A. S. F. would like to thank FAP-DF for providing funding for our research, as well as professors Ricardo Gargano, Bernardo Mello and Luiz Roncaratti for providing important feedback and insights.

Author contribution All authors contributed to the study, conception and design. The first draft of the manuscript was written by Matheus de Oliveira Bispo and Demétrio Antônio da Silva Filho commented on previous versions of the manuscript. All authors read and approved the final manuscript.

Funding D.A.S.F. received financial support from the Edital DPI-UnB No. 02/2021, from CNPq (grants 305975/2019-6, and 420836/2018-7) and FAP-DF (grants 193.001.596/2017 and 193.001.284/2016).

Code and data availability Code and data used are available at https://github.com/m-obispo/lrc-optimization under MIT License.

Declarations

Conflict of interest Not applicable

References

1. Lewars EG (2003) Computational chemistry - introduction to the theory and applications of molecular and quantum mechanics. Kluwer Academic, Tucson, AZ
2. Sun Y, Tsai M, Moe MM, Liu J (2021) Dynamics and multiconfiguration potential energy surface for the singlet O2 reactions with radical cations of guanine, 9-methylguanine, 2'-deoxyguanosine, and guanosine. J. Phys. Chem. A 125(7):1564–1576. https://doi.org/10.1021/acs.jpca.1c00095
3. Mizus II, Kyuberis AA, Zobov NF, Makhnev VY, Polyansky OL, Tennyson J (2018) High-accuracy water potential energy surface for the calculation of infrared spectra. Phil. Trans. R. Soc. A 376(2115):20170149. https://doi.org/10.1098/rsta.2017.0149
4. Bartolomei M, Carmona-Novillo E, Hernández MI, Campos-Martínez J, Moszyński R (2014) Global ab initio potential energy surface for the O2((3)Σ(g)(-)) + N2((1)Σ(g)(-)) interaction. applications to the collisional, spectroscopic, and thermodynamic properties of the complex. J. Phys. Chem. A 118(33):6584–6594. https://doi.org/10.1021/jp503182h
5. Potapov A (March 2017) Weakly bound molecular complexes in the laboratory and in the interstellar medium: A lost interest? Molecular Astrophysics 6:16–21. https://doi.org/10.1016/j.molap.2017.01.001
6. Roncaratti LF, Leal LA, Pirani F, Aquilanti V, e Silva GM, Gargano R (October 2014) Chirality of weakly bound complexes: the potential energy surfaces for the hydrogen-peroxide-noble-gas interactions. J. Chem. Phys. 141(13):134309. https://doi.org/https://doi.org/10.1063/1.4897136
7. Só YAO, Neto PHO, de Macedo LGM, Gargano R (2018) Theoretical investigation on H2O2 (He,Ne, Ar, Kr, Xe, and Rn) complexes suitable for stereodynamics: Interactions and thermal chiral rate consequences. Front. Chem. 6:671. https://doi.org/10.3389/fchem.2018.00671
8. de Araujo Oliveira AL, de Macedo LGM, de Oliveira S YA, Martins JBL, Pirani F, Gargano R (2021) Nature and role of the weak intermolecular bond in enantiomeric conformations of H2O2noble gas adducts: a chiral prototypical model. New J. Chem. 45:8240–8247. https://doi.org/10.1039/D0NJ06135B
9. Palazzetti F, Coletti C, Marrone A, Pirani F (January 2022) Potential energy surfaces for noble gas (Ar, Kr, Xe, Rn)–Propylene Oxide systems: Analytical formulation and binding. Symmetry 14(2):249. https://doi.org/10.3390/sym14020249
10. Amir K, McKemmish LK (2018) Can popular DFT approximations and truncated coupled cluster theory describe the potential energy surface of the beryllium dimer? Aust J Chem 71:804–810. https://doi.org/https://doi.org/10.1071/CH18269
11. Dunning TH (January 1989) Gaussian basis sets for use in correlated molecular calculations. I. the atoms boron through neon and hydrogen. The Journal of Chemical Physics 90(2):1007–1023. https://doi.org/10.1063/1.456153
12. McGuire BA, Carroll PB, Loomis RA, Finneran IA, Jewell PR, Remijan AJ, Blake GA (2016) Discovery of the interstellar chiral molecule propylene oxide (CH3CHCH2O). Science 352(6292):1449–1452. https://doi.org/10.1126/science.aae0328
13. Woods ND, Payne MC, Hasnip PJ (2019) Computing the self-consistent field in kohn–sham density functional theory. J Phys Condens Matter 31(45):453001. https://doi.org/https://doi.org/10.1088/1361-648X/ab31c0
14. Mardirossian N, Head-Gordon M (2017) Thirty years of density functional theory in computational chemistry: an overview and extensive assessment of 200 density functionals. Mol Phys 115(19):2315–2372. https://doi.org/10.1080/00268976.2017.1333644
15. Pereira TL, Leal LA, da Cunha WF, Timteo de Sousa Jnior R, Ribeiro Junior LA, Antonio da Silva Filho D (2017) Optimally tuned functionals improving the description of optical and electronic properties of the phthalocyanine molecule. J Mol Model, 23, https://doi.org/10.1007/s00894-017-3246-7
16. Lima IT, Risko C, Aziz SG, da Silva Filho DA, Brdas JL (2014) Interplay of alternative conjugated pathways and steric interactions on the electronic and optical properties of donoracceptor conjugated polymers. J. Mater. Chem. C 2:8873–8879. https://doi.org/10.1039/C4TC01264J
17. Lima IT, Risko C, Aziz SG, da Silva Filho DA, Brédas JL (2014) Interplay of alternative conjugated pathways and steric interactions on the electronic and optical properties of donor–acceptor conjugated polymers. Journal of Materials Chemistry C 2(42):8873–8879
18. Pandey L, Doiron C, Sears JS, Brdas JL (2012) Lowest excited states and optical absorption spectra of donoracceptor copolymers for organic photovoltaics: a new picture emerging from tuned long-range corrected density functionals. Phys. Chem. Chem. Phys. 14:14243–14248. https://doi.org/https://doi.org/10.1039/C2CP41724C
19. Baer R, Livshits E, Salzner U (2010) Tuned range-separated hybrids in density functional theory. Annu Rev Phys Chem 61(1):85–109. https://doi.org/10.1146/annurev.physchem.012809.103321, PMID: 20055678
20. Chai JD, Head-Gordon M (2008) Systematic optimization of long-range corrected hybrid density functionals. The Journal of Chemical Physics 128(8):084106. https://doi.org/https://doi.org/10.1063/1.2834918
21. Körzdörfer T, Sears J, Sutton C, Brédas JL (2011) Long-range corrected hybrid functionals for π-conjugated systems: Dependence of the range-separation parameter on conjugation length. The Journal of chemical physics 135:204107. https://doi.org/https://doi.org/10.1063/1.3663856
22. Vydrov OA, Scuseria GE (2006) Assessment of a long-range corrected hybrid functional. The Journal of Chemical Physics 125(23):234109. https://doi.org/https://doi.org/10.1063/1.2409292
23. Cabral BJC (2019) The kohn-sham electronic density of states of liquid hcn: Tuning a long-range corrected exchange-correlation functional for predicting electron binding energies. Chem Phys Lett 724:96–102. https://doi.org/https://doi.org/10.1016/j.cplett.2019.03.052
24. Ball R, Brindley J The life story of hydrogen peroxide iii: Chirality and physical effects at the dawn of life. 46, 81–93, https://doi.org/10.1007/s11084-015-9465-y
25. Frisch MJ, Trucks GW, Schlegel HB, Scuseria GE, Robb MA, Cheeseman JR, Scalmani G, Barone V, Petersson GA, Nakatsuji H, Li X, Caricato M, Marenich AV, Bloino J, Janesko BG, Gomperts R, Mennucci B, Hratchian HP, Ortiz JV, Izmaylov AF, Sonnenberg JL, Williams-Young D, Ding F, Lipparini F, Egidi F, Goings J, Peng B, Petrone A, Henderson T, Ranasinghe D, Zakrzewski VG, Gao J, Rega N, Zheng G, Liang W, Hada M, Ehara M, Toyota K, Fukuda R, Hasegawa J, Ishida M, Nakajima T, Honda Y, Kitao O, Nakai H, Vreven T, Throssell K, Montgomery JA, Peralta JE, Ogliaro F, Bearpark MJ, Heyd JJ, Brothers EN,

Kudin KN, Staroverov VN, Keith TA, Kobayashi R, Normand J, Raghavachari K, Rendell AP, Burant JC, Iyengar SS, Tomasi J, Cossi M, Millam JM, Klene M, Adamo C, Cammi R, Ochterski JW, Martin RL, Morokuma K, Farkas O, Foresman JB, Fox DJ (2016) Gaussian16 Revision B.01. Gaussian Inc. Wallingford CT

26. Bokareva OS, Shibl MF, Al-Marri MJ, Pullerits T, Khn O (2017) Optimized long-range corrected density functionals for electronic and optical properties of bare and ligated cdse quantum dots. J Chem Theory Comput 13(1):110–116. https://doi.org/https://doi.org/10.1021/acs.jctc.6b01039. PMID: 27973783
27. Gao F, Han L (2012) Implementing the nelder-mead simplex algorithm with adaptive parameters. Comput Optim Appl 51:259–277. https://doi.org/10.1007/s10589-010-9329-3
28. van der Walt S, Colbert SC, Varoquaux G (2011) The numpy array: A structure for efficient numerical computation. Computing in Science Engineering 13(2):22–30. https://doi.org/https://doi.org/10.1109/MCSE.2011.37
29. Virtanen P, Gommers R, Oliphant TE, Haberland M, Reddy T, Cournapeau D, Burovski E, Peterson P, Weckesser W, Bright J, van der Walt SJ, Brett M, Wilson J, Jarrod Millman K, Mayorov N, Nelson ARJ, Jones E, Kern R, Larson E, Carey CJ, Polat I, Feng Y, Moore EW, Vand erPlas J, Laxalde D, Perktold J, Cimrman R, Henriksen I, Quintero EA, Harris CR, Archibald AM, Ribeiro AH, Pedregosa F, van Mulbregt P, SciPy 1.0 Contributors (2020) SciPy 1.0: Fundamental Algorithms for Scientific Computing in Python. Nat Methods 17:261–272. https://doi.org/https://doi.org/10.1038/s41592-019-0686-2
30. Hunter JD (2007) Matplotlib: A 2d graphics environment. Computing in Science & Engineering 9(3):90–95. https://doi.org/10.1109/MCSE.2007.55